Observations on Return Mapping Algorithms for Piecewise Linear Yield Criteria

Jinsong Huang[1] and D. V. Griffiths[2]

Abstract: This paper shows that for perfect plasticity, the closest point projection method (CPPM) and the cutting plane algorithm (CPA) for return mapping are exactly equivalent for piecewise linear yield criteria under both associated and nonassociated plastic flow. The paper demonstrates this by presenting closed-form expressions for returned stresses in terms of predicted stresses. A consequence of this exact approach is that the final stresses can be obtained in a single iteration. The equivalence of CPPM and CPA is further demonstrated numerically by comparing five previously published algorithms for return mapping to Mohr–Coulomb in a finite-element analysis of bearing capacity. The analyses also highlight issues relating to singularities that occur at the corners of the Mohr–Coulomb surface. It is shown that many of these problems can be avoided if the return mapping is performed in principal stress space as opposed to general stress space.

DOI: 10.1061/(ASCE)1532-3641(2008)8:4(253)

CE Database subject headings: Finite element method; Constitutive models; Elastoplasticity; Geotechnical engineering; Failure investigations; Yield; Algorithms.

Introduction

One of the fundamental ingredients of numerical implementation of plasticity models in geomechanics is numerical integration of the constitutive equations. This integration is carried out locally at each Gauss point in typical finite-element implementations. Generally speaking, these techniques fall into two categories, namely, explicit (forward Euler) and implicit (backward Euler). In the context of implicit integration, the use of return mapping algorithms has become standard nowadays. The return mapping is carried out by first integrating the elastic equations with total strain increments to obtain an elastic stress predictor. These predicted or trial stresses are then relaxed onto a suitably updated yield surface by generating and correcting, iteratively, the plastic strain component of the total strain increments. Among the best-known return mapping algorithms are the radial return method, the closest point projection method (CPPM), and the cutting plane algorithm (CPA). The CPPM is the most commonly used strategy for practical applications (see, e.g., Simo and Taylor 1985 and Simo and Hughes 1998) leading to a nonlinear system of algebraic equations in the stresses and updated internal variables. An iterative algorithm needs to be used to solve these equations, except in the special case of the radial return method for von Mises plasticity (Krieg and Krieg 1977), which leads to a closed-form solution. Bathe et al. (1984) and Kojić and Bathe (1987) introduced the "effective-stress-function" method for the implicit integration of thermoelastoplastic and creep material models (see detail in Bathe 1996; Kojić and Bathe 2005) The algorithm was found to be robust, accurate, and efficient.

Convergence of the CPPM can be a major issue, however, for complex models (e.g., models with highly nonlinear coupling between harding/softening parameters). Difficulty can also be experienced with relatively simple models (e.g., perfect plasticity models) when Gauss point stresses occur in zones of high curvature of the yield function (Ortiz and Popov 1985). In these cases the plastic corrector can have difficulties returning stresses to the yield surface. The numerical results reported by de Souza Neto et al. (1994), Bićanić and Pearce (1996), and Péréz-Foguet et al. (2001) further illustrate these difficulties. Péréz-Foguet et al. (2001) also suggest a substepping scheme along with the corresponding consistent tangent matrix to improve convergence. Caddemi and Martin (1991) show that a line search algorithm may be included to improve convergence when CPPM is implemented with a full Newton–Raphson method. Asensio and Moreno (2003) show that for perfect plasticity with an associated flow rule and an "eikonal" yield surface, the stresses can be returned to the yield surface by an explicit closed-form formula.

Motivated by the work of Krieg and Krieg (1977) and Asensio and Moreno (2003), this paper will show that for perfect plasticity, the trial stresses can be returned to the yield surface using a closed-form expression for both associated and nonassociated flow providing the yield criterion is piecewise linear. Moreover, this paper will show that under such conditions, CPPM and CPA are exactly equivalent.

Piecewise linear yield criteria contain discontinuities in the form of corners in the deviatoric plane and at the apex, so special care has to be taken when the stress point is returned to such a discontinuity. Actually, there are two types of singularity. The first singularity is due to the intersection of linear yield surfaces and can be dealt with using Koiter's theorem (Koiter 1953). Numerous investigators have considered this type of singularity (e.g., de

[1]Assistant Research Professor, Division of Engineering, Colorado School of Mines, Golden, CO 80401. E-mail: jhuang@mines.edu

[2]Professor, Division of Engineering, Colorado School of Mines, Golden, CO 80401 (corresponding author). E-mail: d.v.griffiths@mines.edu

Note. Discussion open until January 1, 2009. Separate discussions must be submitted for individual papers. To extend the closing date by one month, a written request must be filed with the ASCE Managing Editor. The manuscript for this paper was submitted for review and possible publication on July 5, 2007; approved on November 20, 2007. This paper is part of the ***International Journal of Geomechanics***, Vol. 8, No. 4, August 1, 2008. ©ASCE, ISSN 1532-3641/2008/4-253–265/$25.00.

Borst 1987; Larsson and Runesson 1996; Crisfield 1997; Simo and Hughes 1998; Clausen 2006). The second type of singularity is due to undefined derivatives of the yield and potential functions when expressed in general stress space using the invariant J_3 (or the Lode angle). This paper will show that this second type of singularity can lead to serious numerical difficulties when corner solutions are encountered. Returning stresses in principal stress space are recommended because it is shown to avoid entirely the second type of singularity.

Later in this paper a classical bearing capacity analysis will be demonstrated using five typical algorithms that use return mapping to the Mohr–Coulomb yield surface. The algorithms have been implemented in the finite-element framework described by Smith and Griffiths (2004). The results will demonstrate the exact equivalence of CPPM and CPA for piecewise linear yield criteria (such as Mohr–Coulomb) and also the numerical difficulties of returning stresses in a general stress space framework.

Standard Elastoplasticity

This paper will be restricted to small strain, perfect nonassociated plasticity, although the results can easily be extended to associated or linear hardening problems.

The starting point is the fundamental split of the strain rate $\dot{\boldsymbol{\epsilon}}$ into an elastic component $\dot{\boldsymbol{\epsilon}}^e$ and a plastic component $\dot{\boldsymbol{\epsilon}}^p$

$$\dot{\boldsymbol{\epsilon}} = \dot{\boldsymbol{\epsilon}}^e + \dot{\boldsymbol{\epsilon}}^p \tag{1}$$

Based on this decomposition, the elastic stress–strain relationship can be rewritten as

$$\dot{\boldsymbol{\sigma}} = \mathbf{D}^e(\dot{\boldsymbol{\epsilon}} - \dot{\boldsymbol{\epsilon}}^p) \tag{2}$$

where $\mathbf{D}^e$=elastic stress–strain tensor.

Plastic strain rates for nonassociated plasticity are assumed to follow the relations

$$\dot{\boldsymbol{\epsilon}}^p = \dot{\lambda}\mathbf{q} \quad \text{and} \quad \mathbf{q} = \frac{\partial g}{\partial \boldsymbol{\sigma}} \tag{3}$$

where g=plastic potential function; $\dot{\lambda} \geq 0$=consistency parameter, which represents the magnitude of the plastic flow; and $\mathbf{q}$=flow direction given by the derivatives of the plastic potential function g with respect to stress. It is noted that the plastic strain increments are associated with vectors perpendicular to the plastic potential surface.

Loading–unloading conditions are given by the three "Kuhn–Tucker" conditions

$$\dot{\lambda} \geq 0, \quad f \leq 0, \quad \dot{\lambda} f = 0 \tag{4}$$

where $f=f(\boldsymbol{\sigma})$=yield function.

The first condition indicates that the consistency parameter is nonnegative while the second indicates that the stress states must lie on or within the yield surface. The last condition ensures that the stresses lie on the yield surface during plastic loading.

From the loading–unloading conditions, the consistency condition becomes

$$\dot{\lambda}\dot{f} = 0, \quad \text{if } f = 0 \tag{5}$$

hence, if $\dot{\lambda} \neq 0$, then $\dot{f}=0$, that is to say

$$\mathbf{a}^T\dot{\boldsymbol{\sigma}} = 0 \tag{6}$$

$$\mathbf{a}^T\mathbf{D}^e(\dot{\boldsymbol{\epsilon}} - \dot{\boldsymbol{\epsilon}}^p) = 0 \tag{7}$$

$$\mathbf{a}^T\mathbf{D}^e(\dot{\boldsymbol{\epsilon}} - \dot{\lambda}\mathbf{q}) = 0 \tag{8}$$

$$\dot{\lambda} = \frac{\mathbf{a}^T\mathbf{D}^e\dot{\boldsymbol{\epsilon}}}{\mathbf{a}^T\mathbf{D}^e\mathbf{q}} \tag{9}$$

where $\mathbf{a}=(\partial f/\partial \boldsymbol{\sigma})$.

Note that $\mathbf{a}$ and $\mathbf{q}$ are dependent on the stress state, which is dependent on $\dot{\lambda}$ through Eqs. (2) and (3), so Eqs. (2), (3), and (9) are a set of nonlinear equations.

Combining Eqs. (2), (3), and (9) yields the tangential relation between stress and strain rates

$$\dot{\boldsymbol{\sigma}} = \left(\mathbf{D}^e - \frac{\mathbf{D}^e\mathbf{q}\mathbf{a}^T\mathbf{D}^e}{\mathbf{a}^T\mathbf{D}^e\mathbf{q}}\right)\dot{\boldsymbol{\epsilon}} \tag{10}$$

Integration of Eq. (10) leads to the finite-stress increment

$$\Delta\boldsymbol{\sigma} = \int_t^{t+\Delta t}\left(\mathbf{D}^e - \frac{\mathbf{D}^e\mathbf{q}\mathbf{a}^T\mathbf{D}^e}{\mathbf{a}^T\mathbf{D}^e\mathbf{q}}\right)\dot{\boldsymbol{\epsilon}}\mathrm{d}t \tag{11}$$

where t denotes a fictitious time quantity.

From Eq. (10), the continuum elastoplastic modulus $\mathbf{D}^{\mathrm{ep}}$ is defined

$$\mathbf{D}^{\mathrm{ep}} = \mathbf{D}^e - \frac{\mathbf{D}^e\mathbf{q}\mathbf{a}^T\mathbf{D}^e}{\mathbf{a}^T\mathbf{D}^e\mathbf{q}} \tag{12}$$

Integration of Rate Equation by Return Mapping

Return mapping algorithms for integration of Eq. (10) consist of two parts. In the first part, a trial stress increment is computed elastically, and in the second, a correction (or "return") for inelastic behavior is made.

Given the set $(\boldsymbol{\epsilon}_n, \boldsymbol{\epsilon}_n^p, \Delta\boldsymbol{\epsilon})$ at step n and assuming a fully elastic predictor, Eq. (10) can be written as

$$\boldsymbol{\sigma}^{n+1} = \boldsymbol{\sigma}_{n+1}^{\mathrm{trial}} - \mathbf{D}^e\Delta\boldsymbol{\epsilon}_{n+1}^p \tag{13}$$

where

$$\boldsymbol{\sigma}_{n+1}^{\mathrm{trial}} = \boldsymbol{\sigma}_n + \mathbf{D}^e\Delta\boldsymbol{\epsilon} \tag{14}$$

$$\boldsymbol{\sigma}_n = \mathbf{D}^e(\boldsymbol{\epsilon}_n - \boldsymbol{\epsilon}_n^p) \tag{15}$$

$$\Delta\boldsymbol{\epsilon}_{n+1}^p = \int_t^{t+\Delta t}\left(\frac{\mathbf{q}\mathbf{a}^T\mathbf{D}^e}{\mathbf{a}^T\mathbf{D}^e\mathbf{q}}\right)\dot{\boldsymbol{\epsilon}}\mathrm{d}t \tag{16}$$

Note that $\Delta\boldsymbol{\epsilon}$=total strain increment relative to the converged solution from the last load step. This leads to a path-independent strategy, which was first introduced by Bathe et al. (1975). If, on the other hand, $\Delta\boldsymbol{\epsilon}$ is taken as the strain increment between two successive iterations, a path-dependent strategy results, which may cause problems during elastic unloading (see, e.g., Crisfield 1991).

As mentioned before, $\mathbf{a}$ and $\mathbf{q}$ are dependent on the stress state, which in turn is dependent on $\dot{\lambda}$ through Eqs. (2) and (3), so Eq. (16) can be rewritten as

$$\Delta\boldsymbol{\epsilon}_{n+1}^p = \int_{\lambda_n}^{\lambda_{n+1}} m_{\boldsymbol{\sigma}}[\boldsymbol{\sigma}(\dot{\lambda})]\mathrm{d}\dot{\lambda} \tag{17}$$

where $m_{\boldsymbol{\sigma}}$=implicit function of $\dot{\lambda}$.

Ortiz and Popov (1985) considered a generalized form of integration involving adjustable weighting factors $(1-\alpha)$ and α applied to the terms corresponding to the initial and final state, respectively. The generalized trapezoidal rule (GTR) employs the discretized flow rule in the form

$$\Delta\boldsymbol{\epsilon}^p_{n+1} = \Delta\lambda_{n+1}\left\{(1-\alpha)m_{\boldsymbol{\sigma}}[\boldsymbol{\sigma}(\dot{\lambda}_n)] + \alpha m_{\boldsymbol{\sigma}}[\boldsymbol{\sigma}(\dot{\lambda}_{n+1})]\right\} \quad (18)$$

and the generalized midpoint rule (GMR) uses

$$\Delta\boldsymbol{\epsilon}^p_{n+1} = \Delta\lambda_{n+1} m_{\boldsymbol{\sigma}}[(1-\alpha)\boldsymbol{\sigma}(\dot{\lambda}_n) + \alpha\boldsymbol{\sigma}(\dot{\lambda}_{n+1})] \quad (19)$$

where α=weighting factor with the range $0 \le \alpha \le 1$.

Both GTR and GMR lead to a system of nonlinear equations that must be solved iteratively, usually by the Newton method.

Closest Point Projection Method

In the CPPM, the increments of plastic strain are calculated at the end of the step ($\alpha=1$) and the yield condition is enforced at the end of the step. The integration in elastoplastic solutions is always taken over the full load step in each iteration. The integration scheme is written as

$$\boldsymbol{\epsilon}_{n+1} = \boldsymbol{\epsilon}_n + \Delta\boldsymbol{\epsilon} \quad (20)$$

$$\boldsymbol{\epsilon}^p_{n+1} = \boldsymbol{\epsilon}^p_n + \Delta\lambda_{n+1}\mathbf{q}_{n+1} \quad (21)$$

$$\boldsymbol{\sigma}_{n+1} = \mathbf{D}^e(\boldsymbol{\epsilon}_{n+1} - \boldsymbol{\epsilon}^p_{n+1}) \quad (22)$$

$$f_{n+1} = f(\boldsymbol{\sigma}_{n+1}) = 0 \quad (23)$$

which is a system of nonlinear algebraic equations. Eqs. (20)–(23), typically, are linearized using a Newton approach giving rise to a plastic corrector based on the concept of closest point projection. During the plastic-corrector stage of the algorithm, the total strain is constant and linearization is performed with respect to the increment in the plasticity parameter, $\Delta\lambda$.

The notation used in the description of the Newton procedure is as follows: Linearization of $m(\Delta\lambda)=0$ with $\Delta\lambda^{(0)}=0$ at the kth iteration is written as

$$m^{(k)} + \left(\frac{dm}{d\Delta\lambda}\right)^{(k)}\delta\lambda^{(k)} = 0 \quad \text{and} \quad \Delta\lambda^{(k+1)} = \Delta\lambda^{(k)} + \delta\lambda^{(k)} \quad (24)$$

where $\delta\lambda^{(k)}$=increment in $\Delta\lambda$ at the kth iteration. In the following, the load subscript $n+1$ will be omitted, but unless otherwise indicated, all quantities are evaluated at step $n+1$.

Eq. (25) gives the plastic updates and yield condition for Newton iteration as

$$\mathbf{r} = -\boldsymbol{\epsilon}^p + \boldsymbol{\epsilon}^p_n + \Delta\lambda\mathbf{q} = 0$$

$$f = f(\boldsymbol{\sigma}) = 0 \quad (25)$$

which after linearization become

$$\mathbf{r}^{(k)} + [\mathbf{D}^e]^{-1}\Delta\boldsymbol{\sigma}^{(k)} + \Delta\lambda^{(k)}\Delta\mathbf{q}^{(k)} + \delta\lambda^{(k)}\mathbf{q}^{(k)} = 0$$

$$f^{(k)} + \mathbf{a}^{(k)T}\Delta\boldsymbol{\sigma}^{(k)} = 0 \quad (26)$$

where

$$\Delta\mathbf{q}^{(k)} = \frac{\partial\mathbf{q}}{\partial\boldsymbol{\sigma}}^{(k)}\Delta\boldsymbol{\sigma}^{(k)} \quad (27)$$

Substituting Eq. (27) into the first part of Eq. (26) gives

$$\Delta\boldsymbol{\sigma}^{(k)} = -\mathbf{R}^{(k)}\mathbf{r}^{(k)} - \delta\lambda^{(k)}\mathbf{R}^{(k)}\mathbf{q}^{(k)} \quad (28)$$

where

$$\mathbf{R}^{(k)} = \left[\mathbf{I} + \Delta\lambda^{(k)}\mathbf{D}^e\left(\frac{\partial\mathbf{q}}{\partial\boldsymbol{\sigma}}^{(k)}\right)\right]^{-1}\mathbf{D}^e \quad (29)$$

and substituting Eq. (28) into the second part of (26) and solving for $\delta\lambda^{(k)}$ gives

$$\delta\lambda^{(k)} = \frac{f^{(k)} - \mathbf{a}^{(k)T}\mathbf{R}^{(k)}\mathbf{r}^{(k)}}{\mathbf{a}^{(k)T}\mathbf{R}^{(k)}\mathbf{q}^{(k)}} \quad (30)$$

Thus, the plastic strain and the plasticity parameter can be updated as

$$\boldsymbol{\epsilon}^{p(k+1)} = \boldsymbol{\epsilon}^{p(k)} + \Delta\boldsymbol{\epsilon}^{p(k)} = \boldsymbol{\epsilon}^{p(k)} - [\mathbf{D}^e]^{-1}\Delta\boldsymbol{\sigma}^{(k)}$$

$$\Delta\lambda^{(k+1)} = \Delta\lambda^{(k)} + \delta\lambda^{(k)} \quad (31)$$

With the increments as given in Eqs. (28) and (30), the Newton procedure is continued until convergence to the updated yield surface is achieved to within an acceptable tolerance.

Consistent Elastoplastic Modulus

The concept of consistent linearization was first introduced by Bathe et al. (1984); see, also, Kojić and Bathe (1987). To construct the consistent elastoplastic modulus, the change of the stress evaluated by a special return mapping algorithm corresponding to an infinitesimal change of total strain increment is considered. It is different from the continuum elastoplastic modulus, which is obtained by differentiation of the constitutive law. The benefit of using the consistent elastoplastic modulus is that it preserves the quadratic rate of convergence of the Newton–Raphson iterations.

The consistent elastoplastic modulus for the CPPM is defined as

$$\mathbf{D}^{\text{epc}} = \left(\frac{d\boldsymbol{\sigma}}{d\boldsymbol{\epsilon}}\right)_{n+1} \quad (32)$$

To derive an expression for the consistent elastoplastic modulus, Eqs. (20)–(23) can be written in the incremental form (again dropping the subscripts $n+1$)

$$d\boldsymbol{\sigma} = \mathbf{D}^e(d\boldsymbol{\epsilon} - d\boldsymbol{\epsilon}^p) \quad (33)$$

$$d\boldsymbol{\epsilon}^p = d(\Delta\lambda)\mathbf{q} + \Delta\lambda d\mathbf{q} \quad (34)$$

$$df = \mathbf{a}^T d\boldsymbol{\sigma} = 0 \quad (35)$$

where

$$d\mathbf{q} = \left(\frac{\partial\mathbf{q}}{\partial\boldsymbol{\sigma}}\right)d\boldsymbol{\sigma} \quad (36)$$

Substituting Eq. (34) into Eq. (33), using Eq. (36), and solving for $d\boldsymbol{\sigma}$

$$d\boldsymbol{\sigma} = \mathbf{R}d\boldsymbol{\epsilon} - d(\Delta\lambda)\mathbf{R}\mathbf{q} \quad (37)$$

where

$$\mathbf{R} = \left[\mathbf{I} + \Delta\lambda \mathbf{D}^e \left(\frac{\partial \mathbf{q}}{\partial \boldsymbol{\sigma}}\right)\right]^{-1} \mathbf{D}^e \tag{38}$$

Substituting Eq. (37) into the incremental consistency condition (35) and solving for $d(\Delta\lambda)$ gives

$$d(\Delta\lambda) = \frac{\mathbf{a}^T \mathbf{R} d\boldsymbol{\epsilon}}{\mathbf{a}^T \mathbf{R} \mathbf{q}} \tag{39}$$

Substituting this result into Eq. (37)

$$d\boldsymbol{\sigma} = \mathbf{D}^{\text{epc}} d\boldsymbol{\epsilon} \tag{40}$$

gives

$$\mathbf{D}^{\text{epc}} = \mathbf{R} - \frac{\mathbf{R}\mathbf{q}\mathbf{a}^T\mathbf{R}}{\mathbf{a}^T\mathbf{R}\mathbf{q}} \tag{41}$$

which is the so-called consistent elastoplastic modulus.

Cutting Plane Algorithm

An alternative to the CPPM is the cutting plane algorithm presented by Simo and Ortiz (1985) and Ortiz and Simo (1986). The method is based on a steepest descent strategy, which avoids an implicit treatment of the governing equations. The resulting scheme involves an explicit iterative process, thus exhibiting improved convergence properties. The lack of a consistent linearization (see, e.g., Simo and Hughes 1998) in the CPA makes the use of the technique somewhat limited in actual finite-element implementations employing a Newton–Raphson solution strategy. Simo (1998) noted that computational experiments indicated that, in sharp contrast to CPPM, significant errors could result for large load steps; but no details were given.

Using the same return mapping procedure as CPPM, CPA is carried out by first integrating the elastic equations using total strain increments to obtain an elastic predictor. The elastically predicted stresses are then relaxed onto a suitably updated yield surface by correcting iteratively the plastic strain increments. The same steps that led to Eq. (13) in this case give

$$\Delta\boldsymbol{\sigma}^{(k)} = \boldsymbol{\sigma}^{(k+1)} - \boldsymbol{\sigma}^{(k)} = -\mathbf{D}^e \Delta\boldsymbol{\epsilon}^{p(k)} \tag{42}$$

where k=iteration counter.

Defining the flow direction at the initial iterate

$$\Delta\boldsymbol{\epsilon}^{p(k)} = \Delta\lambda^{(k)} \mathbf{q}^{(k)} \tag{43}$$

and substituting into Eq. (42) gives

$$\Delta\boldsymbol{\sigma}^{(k)} = -\Delta\lambda^{(k)} \mathbf{D}^e \mathbf{q}^{(k)} \tag{44}$$

Linearization of the yield function f at each iteration about the current value of stress $\boldsymbol{\sigma}^{(k)}$ leads to

$$f^{k+1} = f^k + \mathbf{a}^{(k)T}(\boldsymbol{\sigma}^{(k+1)} - \boldsymbol{\sigma}^{(k)}) \tag{45}$$

Finally, substitution of Eq. (44) into Eq. (45), and noting that $f^{k+1}=0$ gives

$$\Delta\lambda^{(k)} = \frac{f^{(k)}}{\mathbf{a}^{(k)T}\mathbf{D}^e\mathbf{q}^{(k)}} \tag{46}$$

Equivalence of CPPM and CPA for Piecewise Linear Yield Criteria

In the CPPM method, the flow direction and yield condition are evaluated at the end of the step. As shown in Eq. (29), the gradients of the flow direction need to be computed. In the CPA method, the flow direction is evaluated at the beginning of each iterate. This leads to an explicit algorithm, which requires repeated evaluations of the yield function and the gradients of the yield and plastic potential functions. Simo and Hughes (1998), however, commented that the CPA cannot be exactly linearized. Asensio and Moreno (2003) showed that for associated plastic flow and eikonal yield surfaces, $\mathbf{a}\mathbf{D}^e\mathbf{a}$ is constant, thus the stresses can be returned to the yield surface by an explicit closed-form formula, and an exact form of the consistent tangent moduli can be obtained. This paper will extend this observation to show that for perfectly plastic materials, the trial stress can be returned to the yield surface in closed form for piecewise linear yield criteria under both associated and nonassociated flow. Moreover, it will be shown that under such conditions, CPPM and CPA are exactly equivalent and give exactly the same closed-form expressions.

Return Mapping of Piecewise Linear Yield Criteria in the Case of One Active Yield Surface

Combining Eqs. (2) and (3) gives

$$\boldsymbol{\sigma} = \boldsymbol{\sigma}^{\text{trial}} - \dot{\lambda}\mathbf{D}^e\mathbf{q} \tag{47}$$

and for a convex yield function $f(\boldsymbol{\sigma})$ (see, e.g., Hiriart-Urruty and Lemarachal 1993)

$$\mathbf{a}^T(\boldsymbol{\sigma}^{\text{trial}} - \boldsymbol{\sigma}) \le f(\boldsymbol{\sigma}^{\text{trial}}) \le \mathbf{a}(\boldsymbol{\sigma}^{\text{trial}})^T(\boldsymbol{\sigma}^{\text{trial}} - \boldsymbol{\sigma}) \tag{48}$$

where $\mathbf{a} = \partial f / \partial \boldsymbol{\sigma}$.

Multiplying both terms in Eq. (47) by $\mathbf{a}$ and $\mathbf{a}(\boldsymbol{\sigma}^{\text{trial}})$, we obtain

$$\dot{\lambda}\mathbf{a}^T\mathbf{D}^e\mathbf{q} = \mathbf{a}^T(\boldsymbol{\sigma}^{\text{trial}} - \boldsymbol{\sigma}) \tag{49}$$

$$\dot{\lambda}\mathbf{a}(\boldsymbol{\sigma}^{\text{trial}})^T\mathbf{D}^e\mathbf{q} = \mathbf{a}(\boldsymbol{\sigma}^{\text{trial}})^T(\boldsymbol{\sigma}^{\text{trial}} - \boldsymbol{\sigma}) \tag{50}$$

and combining Eqs. (48)–(50) gives

$$\mathbf{a}^T\mathbf{D}^e\mathbf{q} \le \frac{f(\boldsymbol{\sigma}^{\text{trial}})}{\dot{\lambda}} \le \mathbf{a}(\boldsymbol{\sigma}^{\text{trial}})^T\mathbf{D}^e\mathbf{q} \tag{51}$$

If the yield criterion is piecewise linear and only one yield surface is activated, $\mathbf{a}$ and $\mathbf{q}$ will remain constant during stress return. Thus

$$\mathbf{a}^T\mathbf{D}^e\mathbf{q} = \frac{f(\boldsymbol{\sigma}^{\text{trial}})}{\dot{\lambda}} = \mathbf{a}(\boldsymbol{\sigma}^{\text{trial}})^T\mathbf{D}^e\mathbf{q}(\boldsymbol{\sigma}^{\text{trial}}) \tag{52}$$

and substituting the second equation of Eq. (52) into Eq. (47) gives

$$\boldsymbol{\sigma} = \boldsymbol{\sigma}^{\text{trial}} - \frac{f(\boldsymbol{\sigma}^{\text{trial}})}{\mathbf{a}^T\mathbf{D}^e\mathbf{q}}\mathbf{D}^e\mathbf{q} \tag{53}$$

It should be mentioned that in Eq. (53) both $\mathbf{a}$ and $\mathbf{q}$ can be evaluated at the trial stresses point; thus, the final stress can be obtained explicitly from the trial stress.

Return Mapping of Piecewise Linear Yield Criteria in the Case of Two Active Yield Surfaces

In most cases, there are only two surfaces activated if multisurface return (e.g., return to the corners of Mohr–Coulomb) should be used. The results presented here are easily extended to cases where more than two yield surfaces are active (e.g., return to the apex of Mohr–Coulomb). For determining which yield functions

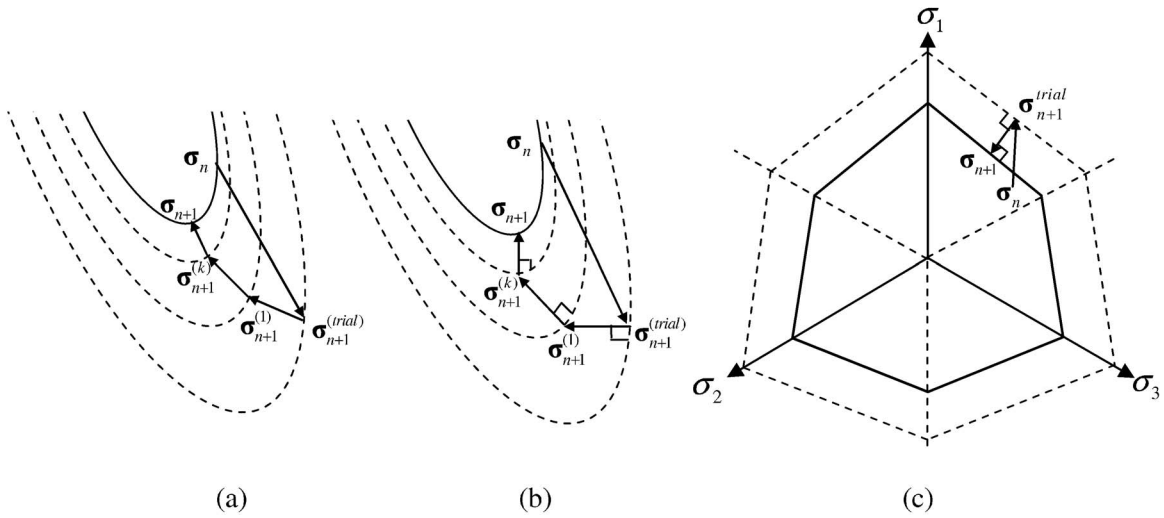

Fig. 1. (a) Stress return corresponding to CPPM; (b) stress return corresponding to CPA; and (c) CPPM and CPA for piecewise linear criteria

are active, readers are referred to Simo and Hughes (1998), de Borst (1987), and Pankaj and Bićanić (1997). This paper will give a brief summary for the case of the Mohr–Coulomb model in the next section.

Koiter (1953) has shown that when two yield functions are active, the plastic strain rate can be written as

$$\dot{\boldsymbol{\epsilon}}^p = \dot{\lambda}_1 \mathbf{q}_1 + \dot{\lambda}_2 \mathbf{q}_2 \tag{54}$$

where $\mathbf{q}_1 = \partial g_1 / \partial \boldsymbol{\sigma}$, $\mathbf{q}_2 = \partial g_2 / \partial \boldsymbol{\sigma}$, and g_1, g_2=plastic potential functions that belong to the active yield functions f_1, f_2; and $\dot{\lambda}_1$, $\dot{\lambda}_2$=two nonnegative plastic multipliers.

The consistency condition in this case can be written as

$$\dot{f}_1 = 0, \quad \dot{f}_2 = 0 \quad \text{if } f_1 = 0, \quad f_2 = 0 \tag{55}$$

and

$$\mathbf{a}_1^T \dot{\boldsymbol{\sigma}} = 0$$

$$\mathbf{a}_2^T \dot{\boldsymbol{\sigma}} = 0 \tag{56}$$

From Eq. (47)

$$\boldsymbol{\sigma} = \boldsymbol{\sigma}^{\text{trial}} - \dot{\lambda}_1 \mathbf{D}^e \mathbf{q}_1 - \dot{\lambda}_2 \mathbf{D}^e \mathbf{q}_2 \tag{57}$$

and for convex yield functions from Eq. (48)

$$\mathbf{a}_1^T (\boldsymbol{\sigma}^{\text{trial}} - \boldsymbol{\sigma}) \le f_1(\boldsymbol{\sigma}^{\text{trial}}) \le \mathbf{a}_1(\boldsymbol{\sigma}^{\text{trial}})^T (\boldsymbol{\sigma}^{\text{trial}} - \boldsymbol{\sigma}) \tag{58}$$

$$\mathbf{a}_2^T (\boldsymbol{\sigma}^{\text{trial}} - \boldsymbol{\sigma}) \le f_2(\boldsymbol{\sigma}^{\text{trial}}) \le \mathbf{a}_2(\boldsymbol{\sigma}^{\text{trial}})^T (\boldsymbol{\sigma}^{\text{trial}} - \boldsymbol{\sigma}) \tag{59}$$

where $\mathbf{a}_1 = (\partial f_1 / \partial \boldsymbol{\sigma})$ and $\mathbf{a}_2 = (\partial f_2 / \partial \boldsymbol{\sigma})$.

Multiplying both sides in Eq. (57) by $\mathbf{a}$ and $\mathbf{a}(\boldsymbol{\sigma}^{\text{trial}})$ and using Eqs. (58) and (59)

$$\mathbf{a}_1^T \mathbf{D}^e (\dot{\lambda}_1 \mathbf{q}_1 + \dot{\lambda}_2 \mathbf{q}_2) \le f_1(\boldsymbol{\sigma}^{\text{trial}}) \le \mathbf{a}_1(\boldsymbol{\sigma}^{\text{trial}})^T \mathbf{D}^e (\dot{\lambda}_1 \mathbf{q}_1 + \dot{\lambda}_2 \mathbf{q}_2) \tag{60}$$

$$\mathbf{a}_2^T \mathbf{D}^e (\dot{\lambda}_1 \mathbf{q}_1 + \dot{\lambda}_2 \mathbf{q}_2) \le f_2(\boldsymbol{\sigma}^{\text{trial}}) \le \mathbf{a}_2(\boldsymbol{\sigma}^{\text{trial}})^T \mathbf{D}^e (\dot{\lambda}_1 \mathbf{q}_1 + \dot{\lambda}_2 \mathbf{q}_2) \tag{61}$$

and since $\mathbf{a}$ and $\mathbf{q}$ are constant

$$f_1(\boldsymbol{\sigma}^{\text{trial}}) = \mathbf{a}_1(\boldsymbol{\sigma}^{\text{trial}})^T \mathbf{D}^e (\dot{\lambda}_1 \mathbf{q}_1 + \dot{\lambda}_2 \mathbf{q}_2) \tag{62}$$

$$f_2(\boldsymbol{\sigma}^{\text{trial}}) = \mathbf{a}_2(\boldsymbol{\sigma}^{\text{trial}})^T \mathbf{D}^e (\dot{\lambda}_1 \mathbf{q}_1 + \dot{\lambda}_2 \mathbf{q}_2) \tag{63}$$

Solving for $\dot{\lambda}_1$, $\dot{\lambda}_2$ from Eqs. (62) and (63)

$$\dot{\lambda}_1 = \frac{c_4 f_1(\boldsymbol{\sigma}^{\text{trial}}) - c_2 f_2(\boldsymbol{\sigma}^{\text{trial}})}{c_1 c_4 - c_2 c_3}$$

$$\dot{\lambda}_2 = \frac{c_1 f_2(\boldsymbol{\sigma}^{\text{trial}}) - c_3 f_1(\boldsymbol{\sigma}^{\text{trial}})}{c_1 c_4 - c_2 c_3} \tag{64}$$

where $c_1 = \mathbf{a}_1^T \mathbf{D}^e \mathbf{q}_1$, $c_2 = \mathbf{a}_1^T \mathbf{D}^e \mathbf{q}_2$, $c_3 = \mathbf{a}_2^T \mathbf{D}^e \mathbf{q}_1$, and $c_4 = \mathbf{a}_2^T \mathbf{D}^e \mathbf{q}_2$, and substituting Eq. (64) into Eq. (57) gives

$$\boldsymbol{\sigma} = \boldsymbol{\sigma}^{\text{trial}} - \frac{c_4 f_1(\boldsymbol{\sigma}^{\text{trial}}) \mathbf{D}^e \mathbf{q}_1 + c_3 f_1(\boldsymbol{\sigma}^{\text{trial}}) \mathbf{D}^e \mathbf{q}_2}{c_1 c_4 - c_2 c_3} + \frac{c_2 f_2(\boldsymbol{\sigma}^{\text{trial}}) \mathbf{D}^e \mathbf{q}_1 + c_1 f_2(\boldsymbol{\sigma}^{\text{trial}}) \mathbf{D}^e \mathbf{q}_2}{c_1 c_4 - c_2 c_3} \tag{65}$$

It can be seen from Eq. (53) that the predicted stresses are returned to the yield surface in closed form as a function of the trial stresses. From Eq. (25) we have $\mathbf{r} = \mathbf{0}$, and thus, Eq. (30), which is the iterative form of the plastic multiplier for CPPM, reduces to Eq. (46) corresponding to CPA. It also can be seen from Eq. (53) that no iterations are needed to get the final stresses.

The equivalence of CPPM and CPA can also be seen in Fig. 1. The CPPM and CPA for general yield surfaces are shown in Figs. 1(a and b), respectively. Note that the flow direction is evaluated at the end of each iteration in CPPM, while CPA evaluates the flow direction at the beginning of each iteration. For piecewise linear criteria, as shown in Fig. 1(c), however, the flow direction corresponding to both the trial state and final states is the same; thus CPPM and CPA are exactly equivalent and only a single iteration is needed for exact return to the yield surface.

Since CPA and CPPM are equivalent for piecewise linear criteria, consistent linearization as described in the section on Consistent Elastoplastic Modulus can be performed. Readers are referred to Larsson and Runesson (1996), Crisfield (1997), Simo and Hughes (1998), Borja et al. (2003), and Clausen (2006) for the case in which two yield surfaces are activated.

Return Mapping to the Mohr–Coulomb Surface

A compression-negative sign convention is assumed throughout, and a stress point in principal stress space is defined using the invariants (see, e.g., Smith and Griffiths 2004)

$$(s,t,\theta) \tag{66}$$

where

$$s = \frac{1}{\sqrt{3}}(\sigma_x + \sigma_y + \sigma_z) \tag{67}$$

$$t = \frac{1}{\sqrt{3}}[(\sigma_x - \sigma_y)^2 + (\sigma_y - \sigma_z)^2 + (\sigma_z - \sigma_x)^2 + 6\tau_{xy}^2 + 6\tau_{yz}^2 + 6\tau_{zx}^2]^{1/2} \tag{68}$$

and

$$\theta = \frac{1}{3}\arcsin\left(\frac{-3\sqrt{6}J_3}{t^3}\right) \tag{69}$$

The third deviatoric stress invariant is given as

$$J_3 = s_x s_y s_z - s_x\tau_{yz}^2 - s_y\tau_{zx}^2 - s_z\tau_{xy}^2 + 2\tau_{xy}\tau_{yz}\tau_{zx} \tag{70}$$

where $s_x=[(2\sigma_x-\sigma_y-\sigma_z)/3]$, etc.

In this notation, s gives the perpendicular distance of the π plane from the origin, and (t,θ) act as polar coordinates within that plane. Those invariants given in expression (66) are favored by the writers because they represent actual lengths in principal stress space.

Other invariants are equally applicable such as

$$\sigma_m = \frac{s}{\sqrt{3}} \tag{71}$$

$$\bar{\sigma} = \sqrt{\frac{3}{2}}t \tag{72}$$

$$I_1 = 3\sigma_m \tag{73}$$

$$J_2 = \frac{t^2}{2} \tag{74}$$

Principal stresses are easily obtained from the invariants as

$$\sigma_1 = \frac{s}{\sqrt{3}} + \sqrt{\frac{2}{3}}t\sin\left(\theta + \frac{2\pi}{3}\right)$$

$$\sigma_2 = \frac{s}{\sqrt{3}} + \sqrt{\frac{2}{3}}t\sin\theta$$

$$\sigma_3 = \frac{s}{\sqrt{3}} + \sqrt{\frac{2}{3}}t\sin\left(\theta - \frac{2\pi}{3}\right) \tag{75}$$

The angular invariant θ from Eq. (69) can be shown to vary in the range $-30° \le \theta \le 30°$.

In terms of principal stresses, the Mohr–Coulomb criterion may be written as

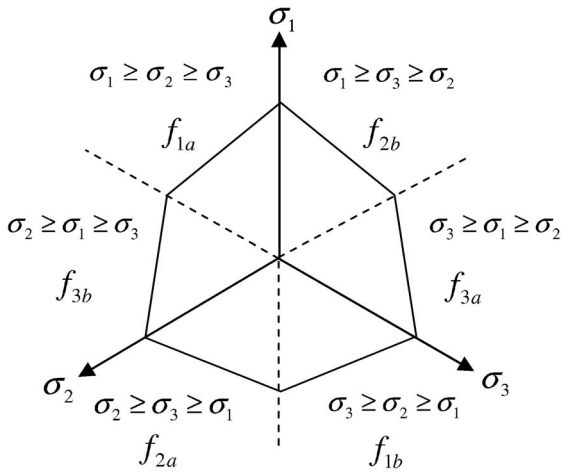

Fig. 2. Mohr–Coulomb surfaces

$$f = \tfrac{1}{2}(\sigma_{\max} - \sigma_{\min}) + \tfrac{1}{2}(\sigma_{\max} + \sigma_{\min})\sin\phi - c\cos\phi \tag{76}$$

where $\sigma_{\max}$ and $\sigma_{\min}$=maximum and minimum principal stresses, respectively; and ϕ and c=familiar friction angle and cohesion of the soil, respectively.

The plastic potential function g is given by replacing the friction angle ϕ by the dilation angle ψ in Eq. (76) and omitting the term $c\cos\psi$.

Looking down the space diagonal, the Mohr–Coulomb surface appears as an irregular hexagon, as shown in Fig. 2.

The six linear portions of the surface depend on the relative size of the principal stresses as indicated, thus

$$f_{1a} = \tfrac{1}{2}(\sigma_1 - \sigma_3) + \tfrac{1}{2}(\sigma_1 + \sigma_3)\sin\phi - c\cos\phi, \quad \text{when } \sigma_1 \ge \sigma_2 \ge \sigma_3 \tag{77}$$

$$f_{1b} = \tfrac{1}{2}(\sigma_3 - \sigma_1) + \tfrac{1}{2}(\sigma_3 + \sigma_1)\sin\phi - c\cos\phi, \quad \text{when } \sigma_3 \ge \sigma_2 \ge \sigma_1 \tag{78}$$

$$f_{2a} = \tfrac{1}{2}(\sigma_2 - \sigma_1) + \tfrac{1}{2}(\sigma_2 + \sigma_1)\sin\phi - c\cos\phi, \quad \text{when } \sigma_2 \ge \sigma_3 \ge \sigma_1 \tag{79}$$

$$f_{2b} = \tfrac{1}{2}(\sigma_1 - \sigma_2) + \tfrac{1}{2}(\sigma_1 + \sigma_2)\sin\phi - c\cos\phi, \quad \text{when } \sigma_1 \ge \sigma_3 \ge \sigma_2 \tag{80}$$

$$f_{3a} = \tfrac{1}{2}(\sigma_3 - \sigma_2) + \tfrac{1}{2}(\sigma_3 + \sigma_2)\sin\phi - c\cos\phi, \quad \text{when } \sigma_3 \ge \sigma_1 \ge \sigma_2 \tag{81}$$

$$f_{3b} = \tfrac{1}{2}(\sigma_2 - \sigma_3) + \tfrac{1}{2}(\sigma_2 + \sigma_3)\sin\phi - c\cos\phi, \quad \text{when } \sigma_2 \ge \sigma_1 \ge \sigma_3 \tag{82}$$

Only yield surface f_{1a} applies if the principal stresses are restricted to $\sigma_1 \ge \sigma_2 \ge \sigma_3$.

When performing return mapping, yield surfaces f_{2b} and f_{3b} will also be involved if the trial stress is located at the corner region. The algorithms to decide which yield surfaces are involved is summarized here.

1. Use Eq. (53) and f_{1a} to get the trial returned stress σ_1^t, σ_2^t, and σ_3^t if $f_{1a} \le 0$ is violated.
2. Check which yield surfaces are involved:

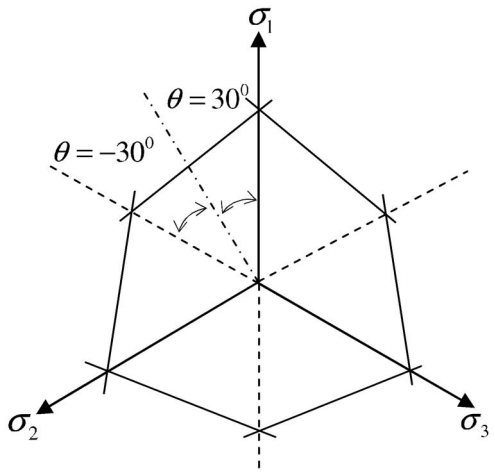

Fig. 3. Singularity of Mohr–Coulomb surfaces due to the intersection of yield surfaces

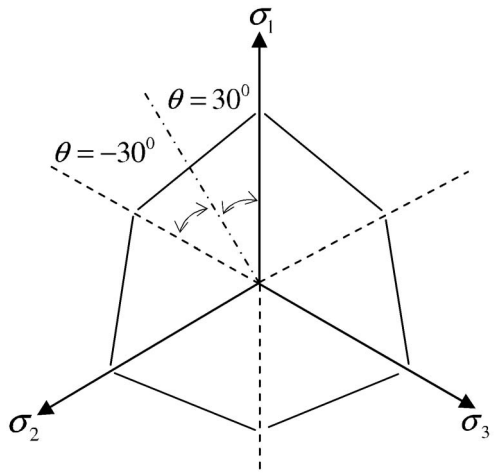

Fig. 4. Singularity of Mohr–Coulomb surfaces due to undefined $\tan 3\theta$ and $1/\cos 3\theta$ (no numerical intersections at corners)

- Case 1: Only one yield surface f_{1a} is involved if $\sigma_1^t \geq \sigma_2^t \geq \sigma_3^t$, σ_1^t, σ_2^t, and σ_3^t are the final returned stresses.
- Case 2: Yield surfaces f_{1a} and f_{2b} are involved if $\sigma_1^t \geq \sigma_3^t \geq \sigma_2^t$. Eq. (65), f_{1a} and f_{2b}, are used to get the final returned stresses.
- Case 3: Yield surfaces f_{1a} and f_{3b} are involved if $\sigma_2^t \geq \sigma_1^t \geq \sigma_3^t$. Eq. (65), f_{1a} and f_{3b}, are used to get the final returned stresses.
- Case 4: Yield surfaces f_{1a}, f_{2b}, and f_{3b} are involved if none of the above conditions are satisfied. The stress will be returned to the apex. The final returned stresses are $\sigma_1 = \sigma_2 = \sigma_3 = c \cot \phi$.

Substitution of the principal stresses from Eq. (75) into the corresponding Mohr–Coulomb surfaces from Eqs. (77), (80), and (82) gives the following expressions in terms of stress invariants:

$$f_{1a} = \frac{s}{\sqrt{3}} \sin\phi + t\left(\frac{\cos\theta}{\sqrt{2}} - \frac{\sin\theta \sin\phi}{\sqrt{6}}\right) - c\cos\phi \tag{83}$$

$$f_{2b} = \frac{s}{\sqrt{3}} \sin\phi + t\left(\frac{\cos\theta}{2\sqrt{2}}(1 + \sin\phi) - \frac{\sin\theta(3 - \sin\phi)}{2\sqrt{6}}\right) - c\cos\phi \tag{84}$$

$$f_{3b} = \frac{s}{\sqrt{3}} \sin\phi + t\left(\frac{\cos\theta}{2\sqrt{2}}(1 - \sin\phi) + \frac{\sin\theta(3 + \sin\phi)}{2\sqrt{6}}\right) - c\cos\phi \tag{85}$$

Return mapping algorithms require evaluation of first derivatives of the yield and potential functions with respect to the stress tensor. In principal stress space, due to isotropy of the involved functions, the return mapping algorithm takes place at a fixed principal axis so that these derivatives of the yield functions and plastic potential functions will remain constant. That is to say, Mohr–Coulomb in principal stress space is piecewise linear. The singularities in this case only arise when two yield surfaces intersect, as shown in Fig. 3. The multisurface plasticity formulation of Koiter (1953) needs to be employed to deal with this type of singularity.

In general stress space, however, the first derivative of any single yield function or plastic potential function with respect to the stress tensor is undefined when $\theta = \pm 30°$. For example,

$$\frac{\partial f_{1a}}{\partial \sigma} = \frac{\partial f_{1a}}{\partial \sigma_m}\frac{\partial \sigma_m}{\partial \sigma} + \frac{\partial f_{1a}}{\partial \theta}\frac{\partial \theta}{\partial J_2}\frac{\partial J_2}{\partial \sigma} + \frac{\partial f_{1a}}{\partial \theta}\frac{\partial \theta}{\partial J_3}\frac{\partial J_3}{\partial \sigma} \tag{86}$$

where

$$\frac{\partial f_{1a}}{\partial \sigma_m} = \sin\phi \tag{87}$$

$$\frac{\partial f_{1a}}{\partial \theta}\frac{\partial \theta}{\partial J_2} = \frac{\partial f_{1a}}{\partial J_2} = \frac{1}{2\sqrt{3J_2}} \cos\theta[\sqrt{3}(1 + \tan\theta \tan 3\theta) + \sin\phi(\tan 3\theta - \tan\theta)] \tag{88}$$

$$\frac{\partial f_{1a}}{\partial \theta}\frac{\partial \theta}{\partial J_3} = \frac{\partial f_{1a}}{\partial J_3} = \frac{\cos\theta}{2J_2 \cos 3\theta}(\sqrt{3}\tan\theta + \sin\phi) \tag{89}$$

It can be seen that when $\theta = \pm 30°$, $\tan 3\theta$ and $1/\cos 3\theta$ in Eq. (88) and (89) are both undefined. The singularities are due to undefined derivatives, not the intersection of yield functions. There are no numerical intersections of yield surfaces in return mapping algorithms, although the intersections actually exist. The gaps between any two yield surfaces as shown in Fig. 4 indicate this type of singularity.

The local rounding technique (e.g., Smith and Griffiths 1988; Abbo and Sloan 1995) must be used to avoid this type of singularity. The local rounding obviously leads to errors, but more seriously, it can cause the yield surface to be highly curved so that the CPPM and CPA may have convergence difficulties. Crisfield's two vector return algorithm (Crisfield 1997) can improve the convergence characteristics of CPPM in these cases; however, it still involves local rounding when the predicted stress is located at corner regions.

Numerical Example

To demonstrate the equivalence of CPPM and CPA for piecewise linear yield criteria, five methods that utilize return mapping are implemented for both associated and nonassociated Mohr–Coulomb within the program structure described in the text by Smith and Griffiths (2004). The first method is a standard CPA in general stress space. Local rounding at the corners uses the method described by Smith and Griffiths (1988). The second

Table 1. Brief Summarization of the Five Methods

Method	Reference	Return mapping method	Working space	Brief description
1	Smith and Griffiths (1988)	CPA	General stress	Local rounding
2	Crisfield (1997)	CPPM	General stress	Two vector return and local rounding
3	de Borst (1987)	CPA/CPPM	Principal stress	Direct integration
4	Larsson and Runesson (1996)	CPPM	Principal stress	Tensor algebra
5	Clausen et al. (2006)	CPPM	Principal stress	Geometrical arguments

method is due to Crisfield (1997) and again involves local rounding with a two vector return strategy based on Koiter's theorem (Koiter 1953). The third method uses the CPA in principal stress space as described by de Borst (1987). The fourth method as described by Larsson and Runesson (1996) uses the CPPM in principal stress space elaborated by tensor algebra. The fifth method also uses the CPPM in principal stress space as described by Clausen (2006) and Clausen et al. (2004, 2005, 2006) but based on geometrical considerations. The five methods used in this paper are summarized in Table 1. It should be mentioned that the standard CPPM in general stress space was attempted by the writers but serious numerical difficulties were encountered for local stress returning. This phenomenon was also observed by several other investigators (e.g., Crisfield 1987; de Souza Neto et al. 1994; Bićanić and Pearce 1996; Péréz-Foguet et al. 2001).

To compare these five methods, a classical footing bearing capacity problem has been analyzed. Both associated and nonassociated flows are considered in order to demonstrate equivalence between CPPM and CPA for piecewise linear yield criteria, two global iterative methods, namely, the modified and full Newton–Raphson methods, were used, together with two global stiffness operators, namely, the continuum and consistent elastoplastic moduli. The modified Newton–Raphson method in this paper uses the elastic global stiffness, which remains constant during iterations and will be referred to as the constant stiffness method.

Fig. 5 shows a mesh involving 32 elements with a flexible strip footing at the surface of a layer of uniform weightless soil. The footing supports a uniform stress q, which is increased incrementally to failure. The mesh consists of eight-noded quadrilateral elements with "reduced" four Gauss-points integration. The elastoplastic soil is described by plane strain Mohr–Coulomb plasticity with $\phi=20°$ and $c=15$ kN/m^2. The dilation angle ψ is set equal to ϕ for associated plastic flow and set to zero for nonassociated plastic flow. The elastic parameters are $E=1\times10^5$ kN/m^2 and $\nu=0.3$ or 0.26. Different Poisson's ratios were implemented to invoke corner solutions at some Gauss points. Theoretically, bearing failure in this problem occurs when q reaches the load given by

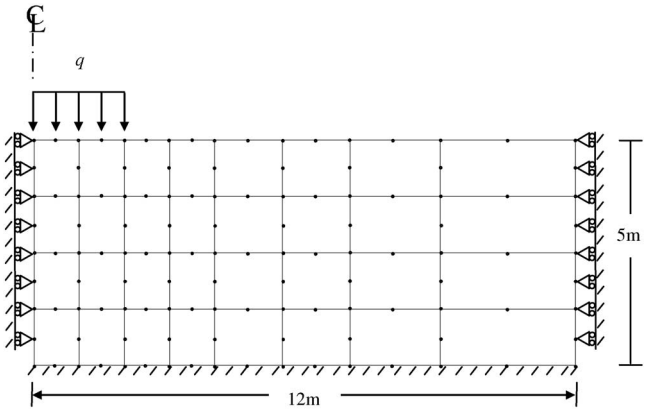

Fig. 5. Mesh of a strip footing

$$q_{\text{ult}} = cN_c \tag{90}$$

where N_c=bearing capacity factor for soil cohesion (Prandtl 1921)

$$N_c = (N_q - 1)\cot\phi \tag{91}$$

where

$$N_q = \tan^2\left(45 + \frac{\phi}{2}\right)e^{\pi\tan\phi} \tag{92}$$

For this particular case, $N_c=14.83$ and $q_{\text{ult}}=222.45$ kN/m^2.

The displacement control can improve the convergence as the global stiffness matrix is not singular at collapse. The load control approach is used because the current algorithm has evolved from slope stability analysis (e.g., Griffiths and Lane 1999), which is strictly load controlled. The convergence of the numerical process to the nonlinear solution is monitored by the condition

$$\frac{\|\mathbf{F}_{\text{ex}} - \mathbf{R}_{\text{in}}\|}{\|\mathbf{F}_{\text{ex}}\|} \le \text{TOL} \tag{93}$$

where TOL=convergence tolerance, which is set to 0.0001; $\mathbf{F}_{\text{ex}}$=total loads applied; and $\mathbf{R}_{\text{in}}$=internal reaction vector evaluated by

$$\mathbf{R}_{\text{in}} = \int\int \boldsymbol{\sigma}\,dxdy \tag{94}$$

The uniform stress q is increased incrementally in 10 load steps to failure. The increments were adjusted manually to be smaller as failure is approaching. Failure is considered to have occurred when the iteration number hits the ceiling as in Tables 2–11 without convergence. The iteration numbers shown in Tables 2–11 are for global force balancing iterations. No substepping scheme was used.

The uniform stress q versus centerline displacements is plotted in Fig. 6. It is seen that q_{ult} for associated plastic flow is between 225 and 230 kN/m^2; q_{ult} for nonassociated plastic flow is between 220 and 225 kN/m^2. Methods 2–5, and Method 1 with no corner solutions ($\nu=0.30$), give the same q_{ult}. Method 1 encountered convergence difficulties when the corner solution were encountered ($\nu=0.26$) and gave lower q_{ult}, as will be described. Fig. 7 shows the deformed mesh and displacement vectors at failure. It is clear that the associated case demonstrates much greater plastic volume change.

The numerical results of all five methods are listed in Tables 2–11. It should be mentioned that corner solutions were encoun-

Table 2. Number of Iterations for Method 1

		$\nu=0.3$		$\nu=0.26$	
Step	q	Continuum	Constant	Continuum	Constant
1	50	2	2	2	2
2	100	6	32	6	38
3	130	5	61	6	79
4	160	5	67	16	79
5	180	5	77	19	83
6	200	5	117	26	127
7	210	4	128	23	132
8	220	6	185	42	239
9	225	8	480	500[a]	5,000[a]
10	230	50[a]	3,000[a]	—	—

Note: CPA with local rounding in general stress space; associated plastic flow.

[a]Failure occurs when the iteration number hits the ceiling.

tered at some Gauss points when $\nu=0.26$ while no corner solutions were found when $\nu=0.30$ in this special problem for both associated and nonassociated flow rules.

In the case where no corner solutions were encountered ($\nu=0.30$) and associated flow, all five implementations gave exactly the same answers with both the continuum or constant stiffness methods as shown in Tables 2, 4, 6, 8, and 10. Of those methods that used a consistent stiffness method, Methods 2 and 4 gave identical results (Tables 4 and 8), but Method 5 gave slightly different results (Table 10) in terms of iterations. When considering nonassociated flow with $\nu=0.30$, Methods 1, 2, 3, and 5 with continuum or constant stiffness gave identical results while Method 4 differed slightly in terms of iterations. All the methods (2, 4, and 5) gave very similar results when the consistent stiffness method was used.

Similar results can be observed from Tables 2 to 11 when corner solutions were encountered ($\nu=0.26$). One exception is that the CPA in general stress apace (Method 1) exhibited convergence difficulties for both associated and nonassociated flow rules due to the local rounding.

It can be concluded from the results listed in Tables 2–11 that CPPM and CPA are equivalent for piecewise linear yield criteria. The slight differences in terms of iterations between the results of these five methods are due to different program implementations and numerical rounding.

The numerical results also show that for Mohr–Coulomb, numerical difficulties can be encountered if the stresses are returned in general stress space and a local rounding is used to avoid a singularity of the gradients of the yield/plastic potential functions (e.g., Methods 1 and 2). The writers, consequently, recommend returning the stresses in principal stress space for Mohr–Coulomb criteria.

Table 3. Number of Iterations for Method 1

		$\nu=0.3$		$\nu=0.26$	
Step	q	Continuum	Constant	Continuum	Constant
1	50	2	2	2	2
2	100	7	32	8	41
3	130	7	62	10	65
4	160	7	72	13	83
5	180	7	76	17	83
6	200	8	115	28	137
7	210	6	168	36	181
8	220	67	4289	500[a]	5,000[a]
9	225	500[a]	5,000[a]	—	—

Note: CPA with local rounding in general stress space; nonassociated plastic flow.

[a]Failure occurs when the iteration number hits the ceiling.

Conclusion

This paper has shown that CPPM and CPA are exactly equivalent for piecewise linear yield criteria under conditions of both associated and nonassociated plastic flow. Closed-form expressions have been provided allowing stress return to be achieved in a single iteration. Numerical results in the analysis of bearing capacity using five different implementations of stress return to the Mohr–Coulomb criterion confirmed the above conclusion, which can readily be extended to cases involving linear isotropic hardening or softening.

A final observation relates to the well-known singularities that occur at the corners of the Mohr–Coulomb surface when computing invariants use general stress terms. It was shown that return algorithms in terms of principal stresses avoid many of these problems.

Table 4. Number of Iterations for Method 2

		$\nu=0.3$			$\nu=0.26$		
Step	q	Consistent	Continuum	Constant	Consistent	Continuum	Constant
1	50	2	2	2	2	2	2
2	100	4	6	32	4	6	38
3	130	4	5	61	4	6	79
4	160	3	5	67	3	6	74
5	180	3	5	77	3	5	81
6	200	3	5	117	4	5	125
7	210	3	4	128	2	4	78
8	220	4	6	185	3	5	197
9	225	4	8	480	4	9	72
10	230	50[a]	50[a]	3,000[a]	50[a]	50[a]	3,000[a]

Note: Crisfield (1997) two vector return in general stress space, CPPM; associated plastic flow.

[a]Failure occurs when the iteration number hits the ceiling.

Table 5. Number of Iterations for Method 2

		$\nu=0.3$			$\nu=0.26$		
Step	q	Consistent	Continuum	Constant	Consistent	Continuum	Constant
1	50	2	2	2	2	2	2
2	100	4	7	32	5	8	41
3	130	4	7	62	4	10	65
4	160	3	7	72	6	8	82
5	180	3	7	76	5	7	84
6	200	3	8	115	3	8	121
7	210	4	6	168	4	6	159
8	220	9	67	4289	8	78	4789
9	225	Diverge	500[a]	5,000[a]	Diverge	500[a]	5,000[a]

Note: Crisfield (1997) two vector return in general stress space, CPPM; nonassociated plastic flow.

[a]Failure occurs when the iteration number hits the ceiling.

Table 6. Number of Iterations for Method 3

		$\nu=0.3$		$\nu=0.26$	
Step	q	Continuum	Constant	Continuum	Constant
1	50	2	2	2	2
2	100	6	32	6	38
3	130	5	61	6	79
4	160	5	67	6	74
5	180	5	77	5	80
6	200	5	117	5	122
7	210	4	128	4	133
8	220	6	185	5	190
9	225	8	480	9	502
10	230	50[a]	3,000[a]	50[a]	3,000[a]

Note: CPA in principal stress space; associated plastic flow.

[a]Failure occurs when the iteration number hits the ceiling.

Table 7. Number of Iterations for Method 3

		$\nu=0.3$		$\nu=0.26$	
Step	q	Continuum	Constant	Continuum	Constant
1	50	2	2	2	2
2	100	7	32	8	41
3	130	7	62	10	65
4	160	7	72	8	81
5	180	7	76	7	84
6	200	8	115	8	127
7	210	6	168	6	182
8	220	67	4,289	74	4,747
9	225	500[a]	5,000[a]	500[a]	5,000[a]

Note: CPA in principal stress space; nonassociated plastic flow.

[a]Failure occurs when the iteration number hits the ceiling.

The five programs used in this paper can be obtained from the corresponding writer.

Acknowledgments

The writers gratefully acknowledge the support of the National Science Foundation under Grant No. CMS-0408150.

Notation

The following symbols are used in this paper:

$\mathbf{a}$ = gradient of yield function respects to stresses;
c = cohesion;
$\mathbf{D}^e$ = elastic stress–strain tensor;
$\mathbf{D}^{\text{ep}}$ = continuum elastoplastic modulus;
$\mathbf{D}^{\text{epc}}$ = consistent elastoplastic modulus;
E = Young's modulus;
$\mathbf{F}_{\text{ex}}$ = external forces;
f = yield function;
g = plastic potential function;
I_1 = first invariant of stress;
J_3 = third deviatoric stress invariant;
k = iteration counter;
$m_{\boldsymbol{\sigma}}$ = implicit function of $\dot{\lambda}$;
N_c = bearing capacity factor for soil cohesion;
n = load step counter;
$\mathbf{q}$ = flow direction;
q = uniform stress;
q_{ult} = bearing capacity;
$\mathbf{R}_{\text{in}}$ = internal reaction;
$\mathbf{r}$ = plastic strain residual;
s = stress invariant, perpendicular distance of the π plane from the origin;
s_x, s_y, s_z = deviatoric stress;
t = fictitious time quantity, stress invariant, perpendicular distance of stress point from the space diagonal;
α = weighting factor $0 \leq \alpha \leq 1$;
θ = stress invariant, Lode angle;
$\Delta\boldsymbol{\epsilon}$ = total strain increment;
$\boldsymbol{\epsilon}$ = strain;
$\dot{\boldsymbol{\epsilon}}$ = strain rate;
$\dot{\boldsymbol{\epsilon}}^e$ = elastic component of strain rate;

Table 8. Number of Iterations for Method 4

		$\nu=0.3$			$\nu=0.26$		
Step	q	Consistent	Continuum	Constant	Consistent	Continuum	Constant
1	50	2	2	2	2	2	2
2	100	4	6	32	4	6	38
3	130	4	5	61	4	6	79
4	160	3	5	67	3	6	74
5	180	3	5	77	3	5	80
6	200	3	5	117	3	5	122
7	210	3	4	128	2	4	133
8	220	4	6	185	3	5	190
9	225	4	8	480	4	9	502
10	230	50[a]	50[a]	3,000[a]	50[a]	50[a]	3,000[a]

Note: Larsson and Runesson (1996) CPPM in principal stress space; associated plastic flow.

[a]Failure occurs when the iteration number hits the ceiling.

Table 9. Number of Iterations for Method 4

		$\nu=0.3$			$\nu=0.26$		
Step	q	Consistent	Continuum	Constant	Consistent	Continuum	Constant
1	50	2	2	2	2	2	2
2	100	4	6	31	4	7	40
3	130	4	7	61	4	9	66
4	160	3	8	69	3	9	80
5	180	3	7	76	3	7	81
6	200	3	8	113	3	9	127
7	210	4	6	150	3	6	163
8	220	8	52	3,156	8	62	3,517
9	225	50[a]	500[a]	5,000[a]	50[a]	500[a]	5,000[a]

Note: Larsson and Runesson (1996) CPPM in principal stress space; nonassociated plastic flow.

[a]Failure occurs when the iteration number hits the ceiling.

Table 10. Number of Iterations for Method 5

		$\nu=0.3$			$\nu=0.26$		
Step	q	Consistent	Continuum	Constant	Consistent	Continuum	Constant
1	50	2	2	2	2	2	2
2	100	5	6	32	5	6	38
3	130	4	5	61	4	6	79
4	160	4	5	67	4	6	74
5	180	4	5	77	4	5	80
6	200	4	5	117	4	5	122
7	210	3	4	128	3	4	133
8	220	4	6	185	4	5	190
9	225	6	8	480	6	9	502
10	230	50[a]	50[a]	3,000[a]	50[a]	50[a]	3,000[a]

Note: Clausen et al. (2006) CPPM in principal stress space; associated plastic flow.

[a]Failure occurs when the iteration number hits the ceiling.

Table 11. Number of Iterations for Method 5

		$\nu=0.3$			$\nu=0.26$		
Step	q	Consistent	Continuum	Constant	Consistent	Continuum	Constant
1	50	2	2	2	2	2	2
2	100	4	7	32	5	8	41
3	130	4	7	62	5	10	65
4	160	4	7	72	4	8	81
5	180	3	7	76	3	7	84
6	200	4	8	115	4	8	127
7	210	4	6	168	4	6	182
8	220	11	67	4,289	11	74	4,747
9	225	Diverge	500[a]	5,000[a]	Diverge	500[a]	5,000[a]

Note: Clausen et al. (2006) CPPM in principal stress space; nonassociated plastic flow.

[a]Failure occurs when the iteration number hits the ceiling.

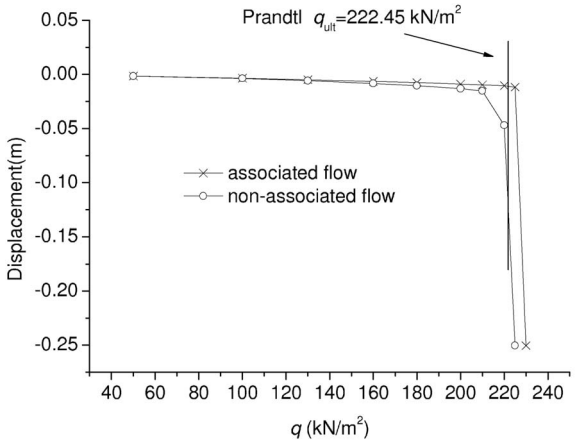

Fig. 6. Pressure versus centerline displacement

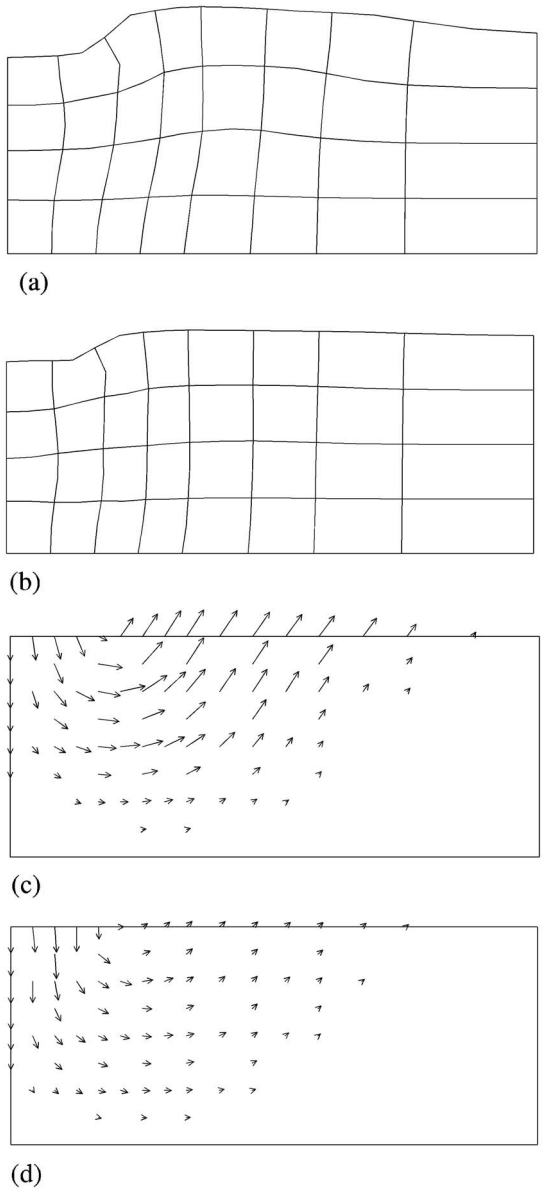

Fig. 7. (a) Deformed mesh (associated plastic flow); (b) deformed mesh (nonassociated plastic flow); (c) displacement vectors at failure (associated plastic flow); and (d) displacement vectors at failure (nonassociated plastic flow)

$\dot{\boldsymbol{\epsilon}}^p$ = plastic component of strain rate;
$\dot{\lambda}$ = consistency parameter;
ν = Poisson's ratio;
$\boldsymbol{\sigma}$ = stress;
σ = normal stress;
$\dot{\boldsymbol{\sigma}}$ = stress rate;
$\bar{\sigma}$ = stress invariant;
$\sigma_1, \sigma_2, \sigma_3$ = principal stresses;
$\sigma_1^t, \sigma_2^t, \sigma_3^t$ = trial returned principal stresses;
σ_m = mean normal stress;
$\sigma_{\max}$ = maximum principal stress;
$\sigma_{\min}$ = minimum principal stress;
$\boldsymbol{\sigma}^{\text{trial}}$ = trial stress;
τ = shear stress;
ϕ = friction angle; and
ψ = dilation angle.

References

Abbo, A. J., and Sloan, S. W. (1995). "A smooth hyperbolic approximation to the Mohr–Coulomb yield criterion." *Comput. Struct.*, 54(3), 427–441.

Asensio, G., and Moreno, C. (2003). "Linearization and return mapping algorithms for elastoplasticity models." *Int. J. Numer. Methods Eng.*, 57(7), 991–1014.

Bathe, K. J. (1996). *Finite-element procedures*, Prentice-Hall, Upper Saddle River, N.J.

Bathe, K. J., Chaudhary, A., Dvorkin, E., and Kojic, M. (1984). "On the solution of nonlinear finite-element equations." *Proc., Int. Conf. on Computer-Aided Analysis and Design of Concrete Structures*, Split, Yugoslavia.

Bathe, K. J., Ramm, E., and Wilson, E. L. (1975). "Finite-element formulations for large deformation dynamic analysis." *Int. J. Numer. Methods Eng.*, 9(2), 353–386.

Bićanić, N., and Pearce, C. J. (1996). "Computational aspects of a softening plasticity model for plain concrete." *Mech. Cohesive-Frict. Mater.*, 1(1), 75–94.

Borja, R. I., Sama, K. M., and Sanz, P. F. (2003). "On the numerical integration of three-invariant elastoplastic constitutive models." *Comput. Methods Appl. Mech. Eng.*, 192(9-10), 1227–1258.

Caddemi, S., and Martin, J. B. (1991). "Convergence of the Newton–Raphson algorithm in elastic–plastic incremental analysis." *Int. J. Numer. Methods Eng.*, 31(1), 177–191.

Clausen, J. (2006). "Efficient nonlinear finite-element implementation of elasto–plasticity for geotechnical problem." Ph.D. thesis, Aalborg Univ.

Clausen, J., Damkilde, L., and Andersen, L. (2004). "One-step direct return method for Mohr–Coulomb plasticity." *Proc., 17th Nordic Seminar of Computational Mechanics*, A. Eriksson, J. Månsson, and G. Tibert, eds., KTH Mechanics, Stockholm, 156–159.

Clausen, J., Damkilde, L., and Andersen, L. (2005). "An efficient return algorithm for nonassociated Mohr–Coulomb Plasticity." *Proc., 10th Int. Conf. on Civil, Structural, and Environmental Engineering Computing*, Rome, 144.

Clausen, J., Damkilde, L., and Andersen, L. (2006). "Efficient return algorithms for associated plasticity with multiple yield planes." *Int. J. Numer. Methods Eng.*, 66(6), 1036–1059.

Crisfield, M. A. (1987). "Plasticity computations using the Mohr–Coulomb yield criterion." *Eng. Comput.*, 4(6), 300–308.

Crisfield, M. A. (1991). *Nonlinear finite-element analysis of solids and structures: Essential*, Vol. 1, Wiley, New York.

Crisfield, M. A. (1997). *Nonlinear finite-element analysis of solids and structures: Advanced topics*, Vol. 2, Wiley, New York.

de Borst, R. (1987). "Integration of plasticity equations for singular yield

functions." *Comput. Struct.*, 26(5), 823–829.
de Souza Neto, E. A., Perić, D., and Owen, D. R. J. (1994). "A model for elastoplastic damage at finite strains: Algorithmic issues and applications." *Eng. Comput.*, 11(3), 257–281.
Griffiths, D. V., and Lane, P. A. (1999). "Slope stability analysis by finite elements." *Geotechnique*, 49(3), 387–403.
Hiriart-Urruty, J. B., and Lemarechal, C. (1993). *Convex analysis and minimization algorithms*, Vol. I., Springer, Berlin.
Koiter, W. T. (1953). "Stress–strain relations, uniqueness, and variational theorems for elastic–plastic materials with a singular yield surface." *Q. Appl. Math.*, 11, 350–354.
Kojić, M., and Bathe, K. J. (1987). "The 'effective-stress-function' algorithm for thermoelastoplasticity and creep." *Int. J. Numer. Methods Eng.*, 24(8), 1509–1532.
Kojić, M., and Bathe, K. J. (2005). *Inelastic analysis of solids and structures*, Springer, Berlin.
Krieg, R. D., and Krieg, D. B. (1977). "Accuracies of numerical solution methods for the elastic–perfectly plastic model." *ASME J. Pressure Vessel Technol.*, 99(4), 510–515.
Larsson, R., and Runesson, K. (1996). "Implicit integration and consistent linearization for yield criteria of the Mohr–Coulomb type." *Mech. Cohesive-Frict. Mater.*, 1(4), 367–383.
Ortiz, M., and Popov, E. P. (1985). "Accuracy and stability of integration algorithms for elastoplastic constitutive relations." *Int. J. Numer. Methods Eng.*, 21(9), 1561–1576.
Ortiz, M., and Simo, J. C. (1986). "An analysis of a new class of integration algorithms for elastoplastic constitutive relations." *Int. J. Numer. Methods Eng.*, 23(3), 353–366.
Pankaj, and Bićanić, N. (1997). "Detection of multiple active yield conditions for Mohr–Coulomb elastoplasticity." *Comput. Struct.*, 62(1), 51–61.
Péréz-Foguet, A., Rodríguez-Ferran, A., and Huerta, A. (2001). "Consistent tangent matrices for substepping schemes." *Comput. Methods Appl. Mech. Eng.*, 190(35-36), 4627–4647.
Prandtl, L. (1921). "über die eindringungsfestigkeit (härte) plastischer baustoffe und die festigkeit von schneiden." *Z. Angew. Math. Mech.*, 1, 15–20.
Simo, J. C. (1998). "Numerical analysis of classical plasticity." *Handbook for numerical analysis*, P. G. Ciarlet and J. J. Lions, eds., Vol. VI, Elsevier, Amsterdam.
Simo, J. C., and Hughes, T. J. R. (1998). *Computational inelasticity*, Springer, New York.
Simo, J. C., and Ortiz, M. A. (1985). "A unified approach to finite deformation elastoplastic analysis based on the use of hyperelastic constitutive equations." *Comput. Methods Appl. Mech. Eng.*, 49(2), 221–245.
Simo, J. C., and Taylor, R. L. (1985). "Consistent tangent operators for rate-independent elastoplasticity." *Comput. Methods Appl. Mech. Eng.*, 48(3), 101–118.
Smith, I. M., and Griffiths, D. V. (1988). *Programming the finite-element method*, 2nd Ed., Wiley, New York.
Smith, I. M., and Griffiths, D. V. (2004). *Programming the finite-element method*, 4th Ed., Wiley, New York.